Magnetic Resonance Imaging 32 (2014) 1058–1066

Contents lists available at ScienceDirect

Magnetic Resonance Imaging

journal homepage: www.mrijournal.com

Non-locally regularized segmentation of multiple sclerosis lesion from multi-channel MRI data

Jingjing Gao [a,b], Chunming Li [b,e,*], Chaolu Feng [c], Mei Xie [a], Yilong Yin [d], Christos Davatzikos [b,e]

[a] School of Electronic Engineering, University of Electronic Science and Technology of China, Chengdu, Sichuan 611731, China
[b] Center of Biomedical Image Computing and Analytics, University of PA, Philadelphia 19104, USA
[c] Key Laboratory of Medical Image Computing of Ministry of Education, Northeastern University, Shenyang, Liaoning 110819, China
[d] School of Computer Science and Technology, Shandong University, Jinan, Shandong 250100, China
[e] Department of Radiology, University of Pennsylvania, Philadelphia, PA 19104, USA

ARTICLE INFO

Article history:
Received 26 August 2013
Revised 20 January 2014
Accepted 7 March 2014

Keywords:
Multi-channel MR images
Lesion segmentation
Energy minimization
Bias field estimation
Nonlocal means

ABSTRACT

Segmentation of multiple sclerosis (MS) lesion is important for many neuroimaging studies. In this paper, we propose a novel algorithm for automatic segmentation of MS lesions from multi-channel MR images (T1W, T2W and FLAIR images). The proposed method is an extension of Li et al.'s algorithm in [1], which only segments the normal tissues from T1W images. The proposed method is aimed to segment MS lesions, while normal tissues are also segmented and bias field is estimated to handle intensity inhomogeneities in the images. Another contribution of this paper is the introduction of a nonlocal means technique to achieve spatially regularized segmentation, which overcomes the influence of noise. Experimental results have demonstrated the effectiveness and advantages of the proposed algorithm.

1. Introduction

Multiple sclerosis (MS) regarded as a white matter disease in young adults is an acquired inflammatory disease of the central nervous system (CNS) of uncertain etiology. It is characterized by demyelination, axonal injury, and gliosis followed by remyelination. MS lesion load and neurodegeneration usually increase with age, and cause focal neurobehavioral syndromes, neuropsychiatric phenomena and dementia [2–5]. Due to the sensitivity of MR image in detecting MS plaques, magnetic resonance imaging (MRI) has become an important paraclinical tool for diagnosing MS. Moreover, the development of immunomodulatory and immunosuppressive therapies also has been critically dependent on MRI, due to the ability of MRI to visualize lesion [6]. MS lesions present as hyper-intensity (WMH) on T2-weighted (T2W) images and fluid attenuated inversion recovery (FLAIR) images, and as hypointense signal on T1-weighted (T1W) images [2]. Quantitative analysis for MR images to measure and monitor lesion load and tissue volumes has become invaluable for patient follow-up and evaluation of therapies [7].

The FLAIR images have similar characteristics with T2W images except for cerebrospinal fluid (CSF) suppression [8,9], which makes the FLAIR image to be more suitable for lesion detection. Therefore, the detection methods of MS lesion are usually optimized for the simultaneous analysis of multiple images, including at least two of T1W, T2W, proton density-weighted (PD), and FLAIR images [10,11]. However, manual delineation of MS lesions is a challenging and time-consuming process, and has poor reproducibility [12]. Furthermore, it usually suffers from significant intra- and inter-observer variation [13]. Therefore, auto-matic lesion segmentation offers an attractive alternative to manual segmentation.

Various supervised MS lesion segmentation algorithms, served as an important kind of automatic lesion segmentation methods, have been presented in recent years. For example, Klöppel et al. [10] separated WMH from intact white matter through the training data, which consists of scans with manually outlined lesions. On the other hand, support-vector machine (SVM) has been applied to detect MS lesions in some supervised lesion segmentation methods. For instance, Lao et al. [14] presented a computer-assisted MS lesion segmentation method based on the local features extracted from multiparametric MRI sequences (T1W, T2W, PD, and FLAIR MRI scans). In this method, an SVM classifier is trained on expert-defined lesions first, and is then employed to classify the new scans. Quddus et al. [15] used the PD scans to generate the simple features, followed

* Corresponding author.
E-mail address: lchunming@gmail.com (C. Li).

http://dx.doi.org/10.1016/j.mri.2014.03.006
0730-725X/

by the radial basis function (RBF) based Adaboost technique and SVM, to segment MS lesions. In addition to the SVM, k-nearest neighbor (k-NN) classification is another supervised learning technique employed as a strategy for lesion segmentation [10]. Anbeek et al. [16,17] performed it to build a feature space from voxel intensities and spatial informations based on T1W, T2W, PD and FLAIR scans for lesion segmentation. Wu et al. [18] also combined an intensity-based statistical k-NN classification with the template-driven segmentation and partial volume artifact correction (TDS+) for segmentation of MS lesion subtypes and brain tissue compartments. Another method proposed by Warfield et al. [19] combined the k-NN classification with nonlinear registration to detect MS lesions.

Apart from the machine learning based lesion segmentation methods, some intensity-based classifiers are employed to detect MS lesions in unsupervised segmentation methods. Gaussian Mixture Model (GMM) is usually employed in lesion segmentation, and MS lesions are segmented as outliers in this model. In [20], Leemput et al. performed intensity-based tissue classification based on a stochastic model of normal brain images, and detected MS lesions as outlier. This method simultaneously corrects image intensity inhomogeneities, estimates tissue-specific intensity models from the data itself, and incorporates contextual information in the classification by Markov random field (MRF). A trimmed likelihood estimator (TLE) is also employed to estimate a GMM from different time points [21]. For example, García-Lorenzo et al. [22] combined TLE with a mean shift algorithm, and Bricq et al. [23] combined it with a Hidden Markov chain to segment MS lesions. In [24], Freifeld et al. performed healthy tissue segmentation according to a probabilistic model of normal brain images, and MS lesions are simultaneously identified as outlier of Gaussian components. The intensity of tissue is considered as a global parameter, and it is constrained to be the same value for a set of related Gaussians per tissue. An active contour algorithm is employed to delineate lesion boundaries. On the other hand, Shi et al. [25] detected lesions within the scope of WM by a coarse-to-fine mathematical morphology method from T1W, FLAIR and diffusion weighted imaging (DWI) sequences.

Some reported methods model MS lesions as a separate class to distinguish from other normal tissues. For instance, Harmouche et al. [26] introduced a fully automatic Bayesian framework into the lesion classification. This method employed posterior probability distributions and entropy values to classify normal and lesion tissue. In [27], a nonstatistical, image-based PVA quantification scheme based on a global edge-based paradigm is applied to segment MS lesions from FLAIR images.

However, progression of MS lesions shows considerable variability. Moreover, temporal changes in MS lesions vary in shape, location and area between patients, even within the same patient [28–31]. For the above reasons, the lesion segmentation results from most reported methods depend on lesion type and imaging modality. Furthermore, noise and residual artifacts in the MR images also make lesion segmentation a challenging problem [6].

In this paper, we proposed a novel algorithm for automatic lesion segmentation from multi-channel MR images (T1W, T2W and FLAIR images) in an energy minimization and nonlocal means framework. This method is an extension of Li et al.'s algorithm in [1], which only segments the normal tissues from T1W images. An energy minimization approach is proposed to segment MS lesions and estimate the bias field from multi-channel images first, and then the nonlocal means is employed to achieve spatially regularized segmentation of MS lesions. The major contributions of this paper can be two-fold. Firstly, MS lesions can be segmented from multi-channel MR images, meanwhile normal tissues are also segmented, and bias field is estimated to handle intensity inhomogeneities in the images. Secondly, a nonlocal means technique is introduced to achieve spatially regularized segmentation and overcome the influence of noise. In addition, the T2W and FLAIR images are rigidly registered to the corresponding T1W images in the preprocessing step.

The remainder parts of this paper are organized as follows: Section 2 expounds the description of our method. We first introduce the vector valued image model and the energy minimization framework to segment MS lesions and estimate bias field. And then, the nonlocal means is introduced to regularize the final lesion segmentation. Experimental results and quantitative evaluations are given in Section 3. Finally, our work is summarized in Section 4.

2. Method

2.1. Image model

Before applying the proposed method, the T2W and FLAIR images are rigidly registered to its corresponding T1W images in the preprocessing step. After registration, the multi-channel MR images are represented as a vector valued image in the image domain Q. The vector valued image can be represented as

$$\mathbf{I}(x) = (I_1(x), \cdots, I_L(x))^T \tag{1}$$

where $I_1(x),\cdots,I_L(x)$ are the MR images in the L channels, and $(\cdot)^T$ is the transpose operator. In this work, three MRI modalities, including T1W, T2W and FLAIR images, are employed to perform lesion segmentation, the L is set to 3 here.

From an accepted model of MR images [32], an MR image $I(x)$ can be decomposed as

$$I(x) = b(x)J(x) + n(x) \tag{2}$$

where $I(x)$ is the observed MR image, $J(x)$ is the true image, $b(x)$ is the bias field, and $n(x)$ is additive noise. In this model, the true image $J(x)$ characterizes a specific physical property of the tissues being imaged, and the bias field $b(x)$ is referred to as spurious smoothly varying image intensities in the image domain.

According to the above MR image model, for each component $I_i(x)$ of the multi-channel MR image $\mathbf{I}(x)$, we have

$$I_i(x) = b_i(x)J_i(x) + n_i(x), \quad i = 1, \cdots, L \tag{3}$$

where $b_i(x), J_i(x)$, and $n_i(x)$ are the bias field, true image, and noise in the i-th channel, respectively.

In this model, the true image in the *i-th* channel, $J_i(x)$, is approximately a constant, $c_{i,j}$, in the j-th tissue region Ω_j due to the physical property of tissues. The constants, $c_{i,1}, \cdots, c_{i,N}$, can be vectorized as $\mathbf{c}_i = (c_{i,1}, \cdots, c_{i,N})^T$ for the i-th channel image. The membership functions, $u_1(x),\cdots, u_N(x)$, are represented as a vector valued membership function $\mathbf{u}(x) = (u_1(x),\cdots, u_N(x))^T$. Thus, the component of the vector valued true image, $J_i(x)$, can be represented as:

$$\begin{aligned} J_i(x) &= \sum_{j=1}^{N} c_{i,j}u_j(x) \\ &= \mathbf{c}_i^T\mathbf{u}(x) \end{aligned} \tag{4}$$

where $u_j(x)$ is the membership function of j-th tissue. For the purpose of lesion segmentation, MS lesions are considered as the fourth type of tissue, in addition to GM, WM, and CSF. Therefore, the N is set to 4 here.

Ideally, every voxel in the image contains only one type of tissue, and the image domain Ω is partitioned into N disjoint tissue regions

$\Omega_1,\ldots,\Omega_N$ for the segmentation purpose. Therefore, the membership function $u_j(x)$ can be either 0 or 1 as

$$\begin{cases} u_j(x) = 1 & x \in \Omega_j \\ u_j(x) = 0 & x \notin \Omega_j \end{cases} \tag{5}$$

However, the N tissues are represented by the fuzzy membership functions with values between 0 and 1 due to the partial volume effect. In this case, one voxel x contains more than one type of tissues, especially, at the interface between neighboring tissues. The fuzzy value of $u_j(x)$ interprets the percentage of j-th tissue within the voxel x. It should satisfy

$$\begin{cases} 0 \le u_j(x) \le 1 & x \in \Omega_j \\ \sum_{j=1}^{N} u_j(x) = 1 \end{cases} \tag{6}$$

Because the bias filed varies smoothly in the image domain, it can be approximated by a linear combination of a set of basis functions, denoted by $g_1(x),\cdots,g_M(x)$, which can be denoted as $G(x) = (g_1(x),\cdots, g_M(x))^T$. Usually, 20 basis functions are used for approximation of bias field in this work. Therefore, the component of the vector valued bias filed $b_i(x)$ can be expressed as

$$b_i(x) \approx \sum_{j=1}^{M} w_{i,j} g_j(x) = \mathbf{w}_i^T G(x) \tag{7}$$

where $w_{i,j}$ is a coefficient of j-th basis function $g_j(x)$ in the i-th channel. The coefficients $w_{i,1},\ldots,w_{i,M}$ are represented by a column vector $\mathrm{w}_i = (w_{i,1},\cdots,w_{i,M})^T$.

2.2. Energy formulation

In this subsection, we extend Li et al.'s formulation for tissue segmentation and bias field estimation in [1] to multi-channel formulation.

According to [1], we first define the following energy for the i-th channel:

$$\mathbf{F}_i(\mathbf{u}, \mathbf{c}_i, \mathbf{w}_i) = \sum_{j=1}^{N} \int_\Omega \left| I_i(x) - b_i(x) c_{i,j} \right|^2 u_j(x) dx, \quad i = 1, \cdots, L \tag{8}$$

From Eqs. (4) and (7), the energy function $\mathbf{F}_i(\mathbf{u}, \mathbf{c}_i, \mathbf{w}_i)$ is rewritten as

$$\mathbf{F}_i(\mathbf{u}, \mathbf{c}_i, \mathbf{w}_i) = \sum_{j=1}^{N} \int_\Omega \left| I_i(x) - \mathbf{w}_i^T G(x) c_{i,j} \right|^2 u_j(x) dx \tag{9}$$

For the multi-channel image $\mathbf{I}(x)$, we define

$$\mathbf{F}(\mathbf{u}, \mathbf{c}, \mathbf{w}) = \sum_{i=1}^{L} \mathbf{F}_i(\mathbf{u}(x), \mathbf{c}_i, \mathbf{w}_i) = \sum_{i=1}^{L} \sum_{j=1}^{N} \int_\Omega \left| I_i(x) - \mathbf{w}_i^T G(x) c_{i,j} \right|^2 u_j(x) dx \tag{10}$$

However, the evaluated membership functions take values either 0 or 1 according to the definition of above energy function. In many applications, it is preferable to obtain a fuzzy or soft segmentation result given by fuzzy membership functions, which take values between 0 and 1. To this end, we introduce a fuzzifier $q > 1$ as in the fuzzy C-means clustering method. We define:

$$\begin{aligned} \mathbf{F}(\mathbf{u}, \mathbf{c}, \mathbf{w}, q) &= \sum_{i=1}^{L} F_i(\mathbf{u}, \mathbf{c}_i, \mathbf{w}_i, q) \\ &= \sum_{i=1}^{L} \sum_{j=1}^{N} \int_\Omega \left| I_i(x) - \mathbf{w}_i^T G(x) c_{i,j} \right|^2 u_j^q(x) dx \end{aligned} \tag{11}$$

where

$$\mathbf{F}_i(\mathbf{u}, \mathbf{c}_i, \mathbf{w}_i, q) = \sum_{j=1}^{N} \int_\Omega \left| I_i(x) - \mathbf{w}_i^T G(x) c_{i,j} \right|^2 u_j^q(x) dx \tag{12}$$

2.3. Energy minimization

An important property of energy $\mathbf{F}(\mathbf{u}, \mathbf{c}, \mathbf{w}, q)$ is that it is convex in each variable. And the energy has a unique minimum point with respect to each variable, respectively. In our method, the optimizations of $\mathbf{u}$, $\mathbf{c}$ and $\mathbf{w}$ are performed by minimizing the energy function in an iterative process. The minimizer of $\mathbf{F}(\mathbf{u}, \mathbf{c}, \mathbf{w})$ in each variable is given below.

Optimization of w

For fixed $\mathbf{c}$ and $\mathbf{u}$, to minimize $\mathbf{F}(\mathbf{u}, \mathbf{c}, \mathbf{w})$ with respect to the variable $\mathbf{w}$, we take derivative of $\mathbf{F}(\mathbf{u}, \mathbf{c}, \mathbf{w}, q)$ with respect to $\mathbf{w}$.

$$\frac{\partial \mathbf{F}(\mathbf{u}, \mathbf{c}, \mathbf{w}, q)}{\partial \mathbf{w}} = 0 \tag{13}$$

It is easy to show that the unique minimizer, denoted by $\hat{\mathbf{w}}_i$, is given by

$$\begin{aligned} \hat{\mathbf{w}}_i &= \mathbf{v}_i^{-1} \mathrm{S}_i \\ &= \left(\int_\Omega G(x) G^T(x) \left(\sum_{j=1}^{N} c_{i,j}^2 u_j^q(x) \right) dx \right) \times \left(\int_\Omega I_i(x) G(x) \left(\sum_{j=1}^{N} c_{i,j} u_j^q(x) \right) dx \right) \end{aligned} \tag{14}$$

where $\mathbf{v}_i$ can be given by

$$\mathbf{v}_i = \left(\int_\Omega G(x) G^T(x) \left(\sum_{j=1}^{N} c_{i,j}^2 u_j^q(x) \right) dx \right)^{-1} \tag{15}$$

and S_i can be given by

$$\mathbf{S}_i = \left(\int_\Omega I_i(x) G(x) \left(\sum_{j=1}^{N} c_{i,j} u_j^q(x) \right) dx \right) \tag{16}$$

With the optimal $\hat{\mathbf{w}}_i$, the bias filed $\hat{b}_i(x)$ is represented as

$$\hat{b}_i(x) = \hat{\mathbf{w}}_i^T G(x) \tag{17}$$

Optimization of c

For fixed $\mathbf{w}$ and $\mathbf{u}$, we can minimize the energy $\mathbf{F}(\mathbf{u}, \mathbf{c}, \mathbf{w})$ with respect to the variable $\mathbf{c}$. The energy $\mathbf{F}(\mathbf{u}, \mathbf{c}, \mathbf{w})$ is rewritten as

$$\begin{aligned} \mathbf{F}(\mathbf{u}, \mathbf{c}, \mathbf{w}, q) &= \sum_{i=1}^{L} \sum_{j=1}^{N} F_{i,j}(\mathbf{u}, \mathbf{c}, \mathbf{w}, q) \\ &= \sum_{i=1}^{L} \sum_{j=1}^{N} \int_\Omega \left| I_i(x) - \mathbf{w}_i^T G(x) c_{i,j} \right|^2 u_j(x)^q dx \end{aligned} \tag{18}$$

where

$$F_{i,j}(\mathbf{u}, \mathbf{c}, \mathbf{w}, \mathrm{q}) = \int_\Omega \left| I_i(x) - \mathbf{w}_i^T G(x) c_{i,j} \right|^2 u_j(x)^q dx \tag{19}$$

where $F_{i,j}(\mathbf{u}, \mathbf{c}, \mathbf{w})$ is the energy of j-th tissue in the i-th channel image.

The minimization of the total energy $\mathbf{F}(\mathbf{u}, \mathbf{c}, \mathbf{w})$ is achieved by minimizing each energy component $F_{i,j}(\mathbf{u}, \mathbf{c}, \mathbf{w})$. We get

$$\frac{\partial F_{i,j}(\mathbf{u}, \mathbf{c}, \mathbf{w}, q)}{\partial c_{i,j}} = 0 \tag{20}$$

Therefore, the estimated intensity mean of j-th tissue in the i-th channel image, $\hat{c}_{i,j}$, can be expressed as

$$\hat{c}_{i,j} = \frac{\int_\Omega b_i(x) I_i(x) u_j^q(x) dx}{\int_\Omega b_i^2(x) u_j^q(x) dx} \tag{21}$$

Optimization of u

By fixing $\mathbf{c}$ and $\mathbf{w}$, we can solve the following constrained energy minimization problem:

$$\hat{\mathbf{u}} = argmin(\mathbf{F}(\mathbf{u}, \mathbf{c}, \mathbf{w}, q)) \tag{22}$$

subject to

$$\sum_{j=1}^{N} u_j(x) = 1, \quad and \quad 0 \le u_j(x) \le 1 \tag{23}$$

It can be shown that the j-th membership function, $\hat{u}_j(x)$, is given by

$$\hat{u}_j(x) = \frac{\left(\sum_{i=1}^{L} \left| I_i(x) - c_{i,j} b_i(x) \right|^2\right)^{\frac{1}{1-q}}}{\sum_{j=1}^{N} \left(\sum_{i=1}^{L} \left| I_i(x) - c_{i,j} b_i(x) \right|^2\right)^{\frac{1}{1-q}}} \tag{24}$$

The optimizations of $\mathbf{c}$, $\mathbf{w}$ and $\mathbf{u}$ are performed in an iterative process for minimizing the energy $\mathbf{F}(\mathbf{u}, \mathbf{c}, \mathbf{w}, q)$. In each iteration, we update each variable with the other two updated in the previous iteration.

2.4. Indirect regularization of membership function by nonlocal means

We note that the formulation of energy $\mathbf{F}(\mathbf{u}, \mathbf{c}, \mathbf{w})$ does not have a mechanism to overcome the influence of MR image noise. In the following subsection, we will describe a strategy to perform the noise reduction.

The nonlocal means (NL-means) filter [33] is introduced in our method to indirectly regularize membership functions in order to overcome the influence of noise.

We define a vector valued function $\mathbf{r}(x)$ as

$$\mathbf{r}(x) \triangleq (r_1(x), \cdots, r_N(x))^T \tag{25}$$

with components

$$r_j(x) \triangleq \sum_{i=1}^{L} \left| I_i(x) - \mathbf{w}_i^T G(x) c_{i,j} \right|^2 \tag{26}$$

The energy function $\mathbf{F}(\mathbf{u}, \mathbf{c}, \mathbf{w})$ can be expressed as a function of the above vector valued function $\mathbf{r}(x)$

$$F(\mathbf{u}, \mathbf{c}, \mathbf{w}) = \int_\Omega \sum_{j=1}^{N} r_j(x) u_j^q(x) dx \tag{27}$$

It can be shown that the j-th tissue membership function $\hat{u}_j(x)$ in $\hat{\mathbf{u}}$ is given by

$$\hat{u}_j(x) = \frac{r_j(x)^{\frac{1}{1-q}}}{\sum_{j=1}^{N} r_j(x)^{\frac{1}{1-q}}} \tag{28}$$

The optimal membership function $\hat{u}_j(x)$ in Eq. (28) can be irregular due to the noise in the image. In this work, we propose to regularize the functions $r_j(x)$, and then compute the membership functions from the regularized functions $\hat{r}_j(x)$. We use the nonlocal means filter to compute the regularized function $\hat{r}_j(x)$ as

$$\hat{r}_j(x) = \frac{1}{Y(x)} \int_\Omega e^{-\frac{\left(G_{\rho *} \left| r(x+\cdot) - r(y+\cdot) \right|^2\right)(0)}{h^2}} r_j(y) dy \tag{29}$$

where $\hat{r}_j(x)$ is the component of the regularized vector valued function $\hat{\mathbf{r}}(x)$, $G\rho$ is the 3-D Gauss kernel with standard deviation ρ, $Y(x)$ is the normalizing factor, and h acts as a filtering parameter

$$G_\rho = \frac{1}{\left(\sqrt[2]{2\pi\rho}\right)^3} e^{-\frac{|x|^2 + |y|^2 + |z|^2}{2\rho^2}} \tag{30}$$

and

$$\begin{aligned} &\left(G_{\rho *} \left| r(x+\cdot) - r(y+\cdot) \right|^2\right)(0) \\ &= \int_{\mathbb{R}^2} G_\rho \left(\sum_{j=1}^{N} \left| r_j(x+l) - r_j(y+l) \right|^2 \right) dl \end{aligned} \tag{31}$$

It can be seen from Eq. (31) that the weights are significant only if a Gaussian window around $r_j(y)$ is similar to the corresponding Gaussian window around $r_j(x)$. $r_j(x)$ is replaced by a weighted average of $r_j(y)$ in Eq. (29).

Given the spatially regularized function $\hat{r}_j(x)$, the final membership function $\tilde{u}_j(x)$ of j-th tissue can be expressed as:

$$\tilde{u}_j(x) = \frac{\hat{r}_j(x)^{\frac{1}{1-q}}}{\sum_{j=1}^{N} \hat{r}_j(x)^{\frac{1}{1-q}}} \tag{32}$$

3. Results and discussions

The proposed method has been tested on the multi-channel images from the MICCAI 2008 MS Lesion Segmentation Challenge [34]. There are 20 training cases which were provided with two sets of manual segmentation from different experts. For all cases, the database contained the same number of high resolution images: T1W, T2W, and FLAIR. The manual segmentations can be viewed as ground truth (GT) to evaluate the automatic lesion segmentation method. Moreover, using more than one set of manual segmentation is very important for evaluating automatic lesion segmentation, since the manual segmentation by different experts shows a large inter-rater variability. In addition, the databases used in the MICCAI 2008 MS Lesion Segmentation Challenge were acquired separately by the Children's Hospital Boston (CHB) and the University of North Carolina (UNC). Ten CHB cases were imaged with 1.5T scanners, whereas the remaining 10 UNC scans were acquired in 3.0T MRI machines.

The T2W and FLAIR images have been rigidly registered to the corresponding T1W images in the image preprocessing step. The fuzzifier of the energy function q is set to 1.5, which is the default value of the parameter in this work.

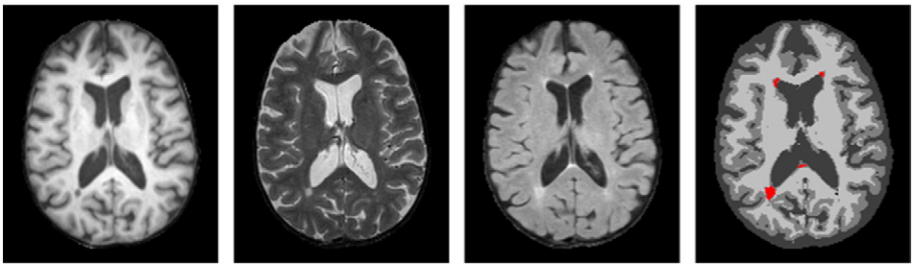

Fig. 1. An example of lesion and normal tissue segmentation by the proposed method. The T1W, T2W, FLAIR images, and the segmentation result are shown from left to right.

3.1. Experimental results

We first show an example of MS lesion and normal tissue segmentation by the proposed method in Fig. 1. The T1W, T2W, FLAIR images, and the segmentation result are shown from left to right. Specifically, the red areas in the fourth column are the lesion segmentation results from our method.

We note that the normal tissue segmentation obtained by our method is not sufficiently accurate, as the contrast between WM and GM in FLAIR images is very low. However, the errors in the normal tissue segmentation do not affect the satisfactory segmentation for MS lesions.

For the sake of comparison, the manual segmentations from two radiologists for four cases are shown in Fig. 2. The FLAIR images, the segmentation results from our method, the first and the second manual segmentations are shown in column 1, 2, 3 and 4, respectively. The red areas in the second column are still the lesion segmentation results from our method; the blue areas and the pink areas in the third and the fourth column are the manual segmentations from the different experts. As shown

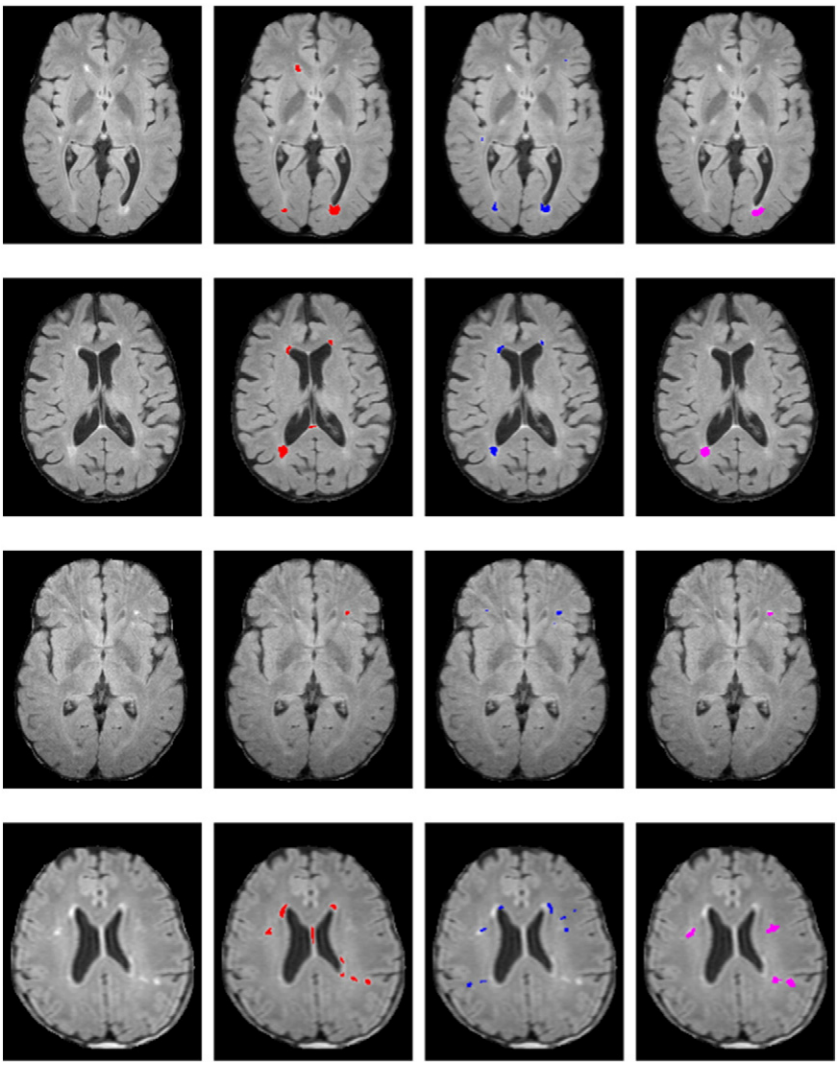

Fig. 2. The comparison results from our method and two manual segmentations. The FLAIR images, the segmentation results from our method, the first and the second manual segmentations are shown from column 1, 2, 3 and 4, respectively.

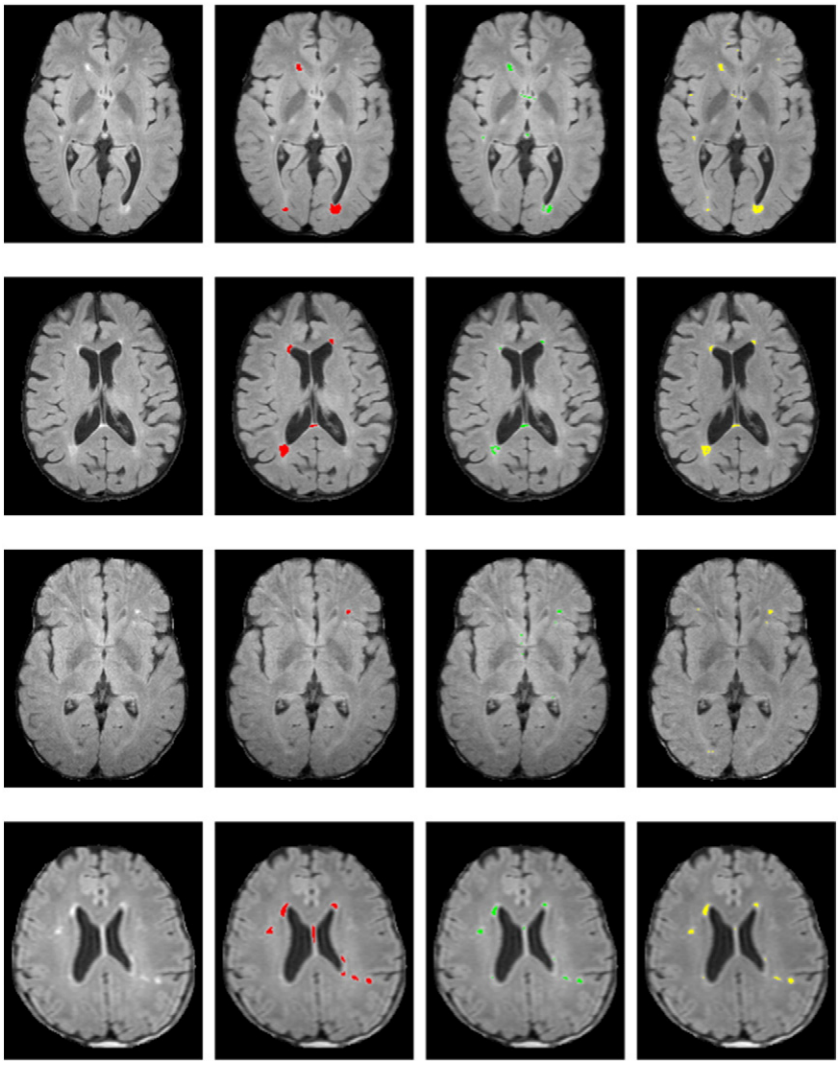

Fig. 3. The comparison results from our method, Leemput et al.'s method and Shiee et al.'s method. The FLAIR images, the segmentation results from our method, Leemput et al.'s method and Shiee et al.'s method are shown from column 1, 2, 3 and 4, respectively.

in this figure, the lesion segmentation results from our method are more accurate than the manual segmentations by the expert radiologists.

We further compared our method with two well known lesion segmentation methods proposed by Leemput et al. [35] and Shiee et al. [7]. The comparison results for some cases are shown in Fig. 3. The

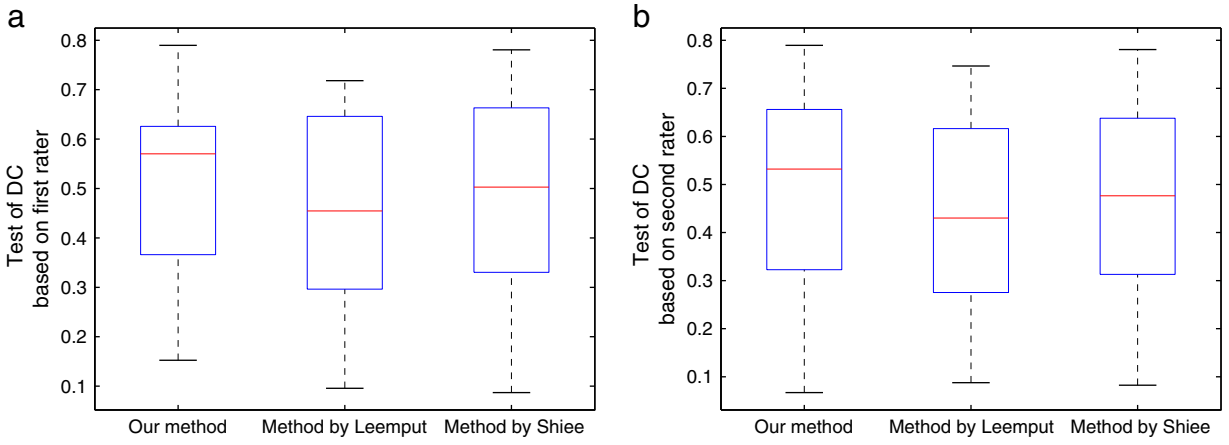

Fig. 4. The comparison of DC value based on two sets of manual segmentation. (a). The comparison of DC value based on the manual segmentation from the first rater; (b). The comparison of DC value based on the manual segmentation from the second rater.

Leemput et al.'s method is implemented by MATLAB functions, which is an add-on to the freely distributed SPM-package. The Shiee et al.'s method is performed by the lesion-TOADS released as plug-ins for the MIPAV software package. The FLAIR images, the segmentation results from our method, Leemput et al.'s method and Shiee et al.'s method are shown in column 1, 2, 3 and 4, respectively. In this figure, the green areas and yellow areas in the third and the fourth column are the segmentation results from Leemput et al.'s method and Shiee et al.'s method. It can be seen from this figure that our method has better performance than the two baseline methods.

3.2. Quantitative evaluation

We first use Dice's coefficient (DC) to measure the similarity of automatic segmentation results and ground truth. For two regions S_1 and S_2, Dice's coefficient is defined as twice the shared information (intersection) over the sum of cardinalities, and calculated based on the similarity of lesion regions [36,37]

$$DC = \frac{2|S_1 \cap S_2|}{|S_1| + |S_2|} \tag{33}$$

The DC values between the results obtained by the three methods and the two manual segmentations are shown in Fig. 4. The comparisons between our method and the two baseline methods based on the first and the second set of manual segmentation are shown in Fig. 4(a) and (b), respectively. It can be seen from this figure that the DC value of our method is higher than those of either the Leemput et al.'s method or the Shiee et al.'s method for both manual segmentations. Thus, our method has better performance than the two baseline methods in terms of DC value.

The specificity [38] indicates the ability of the segmentation to identify negative results. The fewer the number of false positives (FP), the greater value the specificity of the segmentation. It is defined as

$$Specificity = \frac{TN}{TN + FP} \tag{34}$$

where TN is true negative, which is the number of voxels marked as non-MS in both sets, and FP is the false positive, which is the number of voxels only appeared in automatic segmentation.

$$TN = \left|\overline{Ref} \cap \overline{Seg}\right| \tag{35}$$

$$FP = |Seg - Ref| \tag{36}$$

False negative rate (FNR) is the percentage of overestimation (POE) for the results from our method to the manual segmentations. The smaller the FNR value, the more similar the resemblance of automatic segmentation results to the manual segmentations. It is defined as:

$$FNR = \frac{FP}{TN + FP} \tag{37}$$

Table 1
The definitions and evaluation criteria of four metrics for evaluation.

The metrics	Definition	Best	Worst
DC	$\frac{2\|S_1 \cap S_2\|}{\|S_1\|+\|S_2\|}$	1	0
Specificity	$\frac{TN}{TN+FP}$	1	0
FNR	$\frac{FP}{TN+FP}$	0	1
VD	$\frac{Vol(Seg)-Vol(GT)}{Vol(GT)}$	0	$<\infty$

Table 2
The detail index of our method with two sets of manual segmentation, including specificity, FNR and VD.

Ground truth	Rater 1			Rater 2		
All database	Specificity	FNR [%]	VD [%]	Specificity	FNR [%]	VD [%]
Case 01	0.9907	0.1135	72.4035	0.9807	0.0535	69.3340
Case 02	0.9993	0.0748	20.2244	0.9893	0.0948	17.1549
Case 03	0.9992	0.0845	26.2230	0.9892	0.1045	23.1535
Case 04	0.9992	0.0812	21.5576	0.9892	0.1012	18.4881
Case 05	0.9975	0.2526	40.8066	0.9875	0.2726	37.7371
Case 06	0.9964	0.3559	37.4234	0.9864	0.3759	34.3539
Case 07	0.9986	0.1379	22.0240	0.9886	0.1579	18.9545
Case 08	0.9973	0.2693	25.3970	0.9873	0.2893	22.3275
Case 09	0.9984	0.1550	31.8845	0.9884	0.1750	28.8150
Case 10	0.9989	0.1135	38.0539	0.9889	0.1335	34.9844
Case 11	0.9987	0.1345	226.7548	0.9984	0.1582	50.0613
Case 12	0.9989	0.1119	34.9856	0.9987	0.1276	65.6684
Case 13	0.9987	0.1258	151.7606	0.9989	0.1109	44.6996
Case 14	0.9986	0.1384	82.1644	0.9991	0.0948	41.3029
Case 15	0.9999	0.0125	166.6667	0.9999	0.0075	18.3074
Case 16	0.9984	0.1604	50.4961	0.9974	0.2564	139.5128
Case 17	0.9983	0.1687	274.6231	0.9983	0.1703	77.7605
Case 18	0.9996	0.0385	138.5135	0.9997	0.0345	37.3813
Case 19	0.9994	0.0553	332.5792	0.9997	0.0315	23.0430
Case 20	0.9985	0.1518	207.1048	0.9989	0.1140	74.3306

Volume difference (VD) evaluates the differences between the automatic segmentation (Seg) and ground truth (GT) by computing their volume (Vol). It is defined as:

$$VD = \frac{Vol(Seg) - Vol(GT)}{Vol(GT)} \tag{38}$$

For lesion segmentation, the manual segmentation is used as GT to evaluate the VD value. Even though the manual segmentations cannot be considered to be 100% ground truth, they are still a good way of comparing the automatic lesion segmentation. A smaller VD value suggests a better automatic segmentation result.

The definitions and evaluation criteria of these indexes are summarized in Table 1.

We tested specificity, false negative rate and volume difference for the 20 sets of multi-channel MR images. The results of these indexes are listed in Table 2. It can be seen that the specificity value of our method to the 20 cases approaches 1 for both sets of manual segmentation. Thus, our method has a very low false positive rate. Furthermore, our method also has a very low FNR value. Therefore, the lesion segmentation results from our method are similar to the manual segmentations for most of cases. Finally, it can be seen from the table that our method also has a very low VD value for the two sets of manual segmentation.

In order to further compare with the two sets of manual segmentation and two baseline methods, we randomly choose 60 slices from the 20 cases, and invite a radiologist to evaluate our segmentation results by giving a performance score for each slice. The meaning of score, such as 2, 1, 0, −1, −2, is given in Table 3. Fig. 5 shows the performance comparison between our method, two

Table 3
The meaning of score.

The score	The signification of score
−2	much worse
−1	worse
0	similar
+1	better
+2	much better

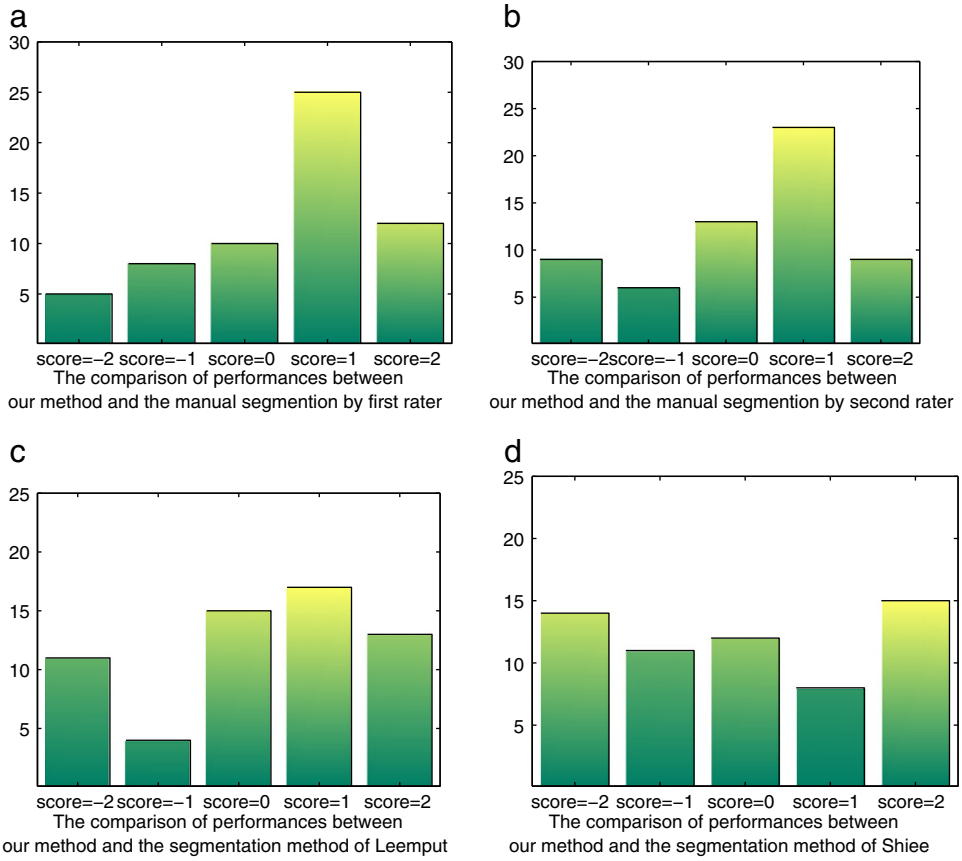

Fig. 5. The score of our method comparing with the two sets of manual segmentation, Leemput et al.'s method and Shiee et al.'s method, respectively. (a). The score of our method comparing with the manual segmentation acquired by the first rater; (b). The score of our method comparing with the manual segmentation acquired by the second rater; (c). The score of our method comparing with the Leemput et al.'s method. (d). The score of our method comparing with the Shiee et al.'s method.

sets of manual segmentation and two baseline algorithms, respectively. According to the evaluation of radiologist, our method has better performance than either the two manual segmentations or the baseline methods, as can be seen in this figure.

4. Conclusion

In this paper, we have presented a new method for MS lesion segmentation from multi-channel MR images. The proposed method first performs the preliminary segmentation of MS lesions and estimation of bias field in an energy minimization framework, and then it introduces a nonlocal means technique to achieve spatially regularized segmentation. Quantitative evaluation and comparison with two well known methods have demonstrated the superior performance of our method in terms of segmentation accuracy.

References

[1] Li C, Gatenby C, Wang L, Gore JC. A robust parametric method for bias field estimation and segmentation of mr images. Computer Vision and Pattern Recognition, 2009, CVPR 2009. IEEE Conference on, IEEE; 2009. p. 218–23.
[2] Schmahmann JD, Smith EE, Eichler FS, Filley CM. Cerebral white matter. Ann N Y Acad Sci 2008;1142(1):266–309.
[3] Prins ND, van Straaten EC, van Dijk EJ. 3d segmentation in the clinic: a grand challenge ii: Ms lesion segmentation. MIDAS J 2004;62(9):1522–39.
[4] Wahlund LO, Barkhof F, Fazekas F. A new rating scale for age-related white matter changes applicable to mri and ct. Stroke 2001;32:1318–22.
[5] Scheltens P, Barkhof F, Leys D. A semiquantative rating scale for the assessment of signalhyperintensities on magneticresonanceimaging. J Neurol Sci 1993;114(1):7–12.
[6] D. Garcla-Lorenzo, S. Francis, S. Narayanan, D. L. Arnold, D. Louis Collins, Review of automatic segmentation methods of multiple sclerosis white matter lesions on conventional magnetic resonance imaging, Medical image analysis, 2013.
[7] Shiee N, Bazin P-L. A semiquantative rating scale for the assessment of signalhyperintensities on magneticresonanceimaging. NeuroImage 2010;49(1):1524C–35C.
[8] Hirono N. Impact of white matter changes on clinical manifestation of Alzheimer's disease: a quantitative study. Stroke 2000;31:2182–8.
[9] Jr C. Flair histogram segmentation for measurement of leukoaraiosis volume. Magn Reson Imaging 2001;14:668–76.
[10] Klöppel S, Abdulkadir A, Hadjidemetriou S, Issleib S, Frings L, Thanh TN, et al. A comparison of different automated methods for the detection of white matter lesions in mri data. NeuroImage 2011;57(2):416–22.
[11] Llado X, Oliver A, Cabezas M, Freixenet J, Vilanova JC, Quiles A, et al. Segmentation of multiple sclerosis lesions in brain mri: a review of automated approaches. Inf Sci 2012;186(1):164–85.
[12] Yamamoto D, Arimura H, Kakeda S. Computer-aided detection of multiple sclerosis lesions in brain magnetic resonance images: false positive reduction scheme consisted of rule-based, level set method, and support vector machine. Comput Med Imaging Graph 2010;34(5):404C–13C.
[13] Breiman L. Random forests. Mach Learn 2001;45(1):5–32.
[14] Lao Z, Shen D. Computer-assistedsegmentation of white matter lesions in 3d mr images using support vector machine. Acad Radiol 2008;15(3):300C–13C.
[15] Quddus A, Fieguth P. Adaboost and support vector machines for white matter lesion segmentation in mr images. Shanghai 2005;1:463–6.
[16] Anbeek P, Vincken KL. Automatic segmentation of different-sized white matter lesions by voxel probability estimation. Med Image Anal 2004;8(3):205C–15C.
[17] Anbeek P, Vincken KL. Probabilistic segmentation of white matter lesions in mr imaging. NeuroImage 2004;21(3):1318C–22C.
[18] Wu Y, Warfield SK. Automated segmentation of multiple sclerosis lesion subtypes with multichannel mri. NeuroImage 2006;32(3):1205C–15C.
[19] Warfield S, Kaus M. Adaptive, template moderated, spatially varying statistical classification. Med Image Anal 2000;4(3):677C–88C.
[20] Leemput KV, Maes F, Vandermeulen D, Colchester A. Automated segmentation of multiple sclerosis lesions by model outlier detection. IEEE Trans Med Imaging 2001;20(8):677C–88C.
[21] Ait-Ali L, Prima S, Hellier P, Carsin B, Edan GG, Barillot C. Strem: a robust multidimensional parametric method to segment ms lesions in mri. MICCAI'05; 2005. p. 409–16.
[22] García-Lorenzo D, Prima S, Collins D. Combining robust expectation maximization and mean shift algorithms for multiple sclerosis brain segmentation. MCCAI'08; 2008. p. 82–91.

[23] Bricq S, Collet C, Armspach JP. Lesion detection in 3d brain mri using trimmed likelihood estimator and probabilistic atlas. ISBI'08; 2008. p. 93–6.
[24] Freifeld O, Greenspan H, Goldberger J. Lesion detection in noisy mr brain images using constrained gmm and active contours. ISBI'07; 2007. p. 596–9.
[25] L. Shi, D. Wang, S. Liu, Y. Pu, Y. Wang, W. C. Chu, A. T. Ahuja, Y. Wang, Automated quantification of white matter lesion in magnetic resonance imaging of patients with acute infarction, Journal of neuroscience methods, 2013.
[26] Harmouche R, Collins L, Arnold D, Francis S, Arbel T. Bayesian ms lesionclassification modeling regional and local spatial information. ICPR'06; 2006. p. 984–7.
[27] Khademi A, Venetsanopoulos A, Moody AR. Robust white matter lesion segmentation in flair mri, biomedical engineering. IEEE Trans 2012;59(3):860–71.
[28] Wallace CJ, Seland TP, Fong TC. Multiple sclerosis: the impact of mr imaging. Am J Roentgenol 1992;158(1):849–57.
[29] Wiebe S, Lee DH, Karlik SJ, Hopkins M, Vandervoort MK. Serial cranial and spinal cord magnetic resonance imaging in multiple sclerosis. Ann Neurol 1992;32:643–50.
[30] Truyen L. Magnetic resonance imaging in multiple sclerosis: a review. Acta Neurol Belg 1994;94(1):98–102.
[31] Fazekas F, Barkhof F, Filippi M, Grossman RI, Li DK. The contribution of magnetic resonance imaging to the diagnosis of multiple sclerosis. Neurology 1999;53(1):448–56.
[32] Pham DL, Prince JL. Adaptive fuzzy segmentation of magnetic resonance images. IEEE Trans Med Imaging 1999;18(9):737–52.
[33] Buades A, Coll B, Morel J-M. Nonlocal image and moive denoising. Int J Comput Vis 2008;76:123–39.
[34] Styner MW, Niessen S, Walsum WV, Metz T, Schaap C, Deng M, et al. Ms lesion segmentation, challenge; 2008.
[35] Van Leemput K, Maes F, Bello F, Vandermeulen D, Colchester A, Suetens P. Automated segmentation of ms lesions from multichannel mr images. Medical Image Computing and Computer-Assisted Intervention-MICCAI99. Springer; 1999. p. 11–21.
[36] Collins DL, Zijdenbos AP, Kollokian VV. Design and construction of a realistic digital brain phantom. IEEE Trans Med Imaging 1999;17(3):463–8.
[37] Kwan RK-S, Evans AC, Pike GB. An extensible mri simulator for post-processing evaluation. Lect Notes Comput Sci 1996;1131:135–40.
[38] Richard Sims VG. Aurelie Isambert, A pre-clinical assessment of an atlas- based automatic segmentation tool for the head and neck. Radiother Oncol 2009;93:474–8.